Tunable Dispersion and Supercontinuum Generation in Disordered Glass-Air Anderson Localization Fiber

Stefan Gausmann, Xiaowen Hu, Jian Zhao, Md. Selim Habib, *Senior Member, IEEE, Senior Member, OSA*, He Cheng, J. E. Antonio-Lopez, Xiaoming Yu, Rodrigo Amezcua-Correa, *Member, IEEE, Member, OSA*, and Axel Schülzgen, *Fellow, IEEE, Fellow, OSA*

***Abstract*—In this paper, we discuss chromatic dispersion properties of transverse Anderson localization optical fiber (TALOF) and their implications on broad band supercontinuum (SC) generation. Our dispersion study reveals a clear correlation between the Anderson localization length and the dispersion properties of highly localized TALOF modes. We demonstrate that the zero dispersion wavelength can be tuned over more than 300 nm within the same fiber by selected excitation of specific modes. We exploit this unique TALOF property, which we validated with rigorous finite-element modeling, to generate multi octave spanning SC ranging from 460–1750 nm, highlighting the great potential of disordered Anderson localization fibers for nonlinear applications.**

***Index Terms*—Hollow-core anti-resonant fiber, ultrafast nonlinear dynamics, higher-order modes, dispersive wave.**

I. Introduction

TRANSVERSE Anderson localization in optics is a remarkable phenomenon and describes the confinement of light in a dielectric medium with a transverse random and longitudinal uniform refractive index distribution [1], [2], [3], [4]. This localization effect is caused by strong scattering of light in the transverse direction and leads to the formation of so called Anderson-modes that can propagate freely in the invariant longitudinal direction [5], [6], [7], [8]. The observation of Anderson-modes in one and two dimensional optical systems has triggered the development of a novel fiber class that relies on random refractive index distributions instead of traditional core cladding structures to guide light [9], [10], [11], [12], [13]. The localized modes in Transverse Anderson localization fibers (TALOFs) have demonstrated exceptional and to some degree counter intuitive properties, such as disorder-induced single mode transmission with low propagation loss as well as high resiliency to fiber bending [14], high quality wave fronts [15], and a weak wavelength-dependency of the mode size [16], [17]. These unique TALOF properties have been successfully exploited for applications such as high quality image transport [13], [18], [19], [20], [21], light focusing [22], [23], quantum key distribution [24], random lasing [25], and four wave mixing [26]. To expand the current application space of TALOFs into novel as well as classical fiber domains such as optical communication [27] or nonlinear optics [26], the understanding of fundamental fiber properties such as the chromatic dispersion of Anderson-modes is crucial. Therefore, we present here a detailed study on the chromatic dispersion properties of highly localized Anderson-modes guided in a glass-air TALOF. The modal properties of the fiber were calculated using finite-element method (FEM) based on Comsol Multiphysics. Our dispersion measurements as well as our rigorous simulations reveal that the zero dispersion wavelength of highly localized Anderson-modes is strongly correlated with the Anderson localization length and can be widely tuned by changing the mode excitation conditions. We exploited this unique property of our glass-air TALOF for multi-octave spanning supercontinuum (SC) generation by selectively exciting an Anderson-mode with high anomalous dispersion at the emission wavelength of our fs-pump laser.

Manuscript received 28 September 2022; revised 29 November 2022; accepted 1 December 2022. Date of publication 23 December 2022; date of current version 17 April 2023. The work of Md. Selim Habib was supported by Woodrow W. Everett, Jr. SCEEE Development Fund in cooperation with the Southeastern Association of Electrical Engineering Department Heads. This work was supported in part by the National Science Foundation (NSF) under Grant ECCS-1711230, in part by Army Research Office (ARO) under Grants W911NF-19-1-0426, W911NF-17-1-0501, and W911NF-12-1-0450, and in part by the Air Force Office of Scientific Research (AFOSR) under Grants FA9550-15-1-0041 and FA8651-18-20019. *(Corresponding author: Stefan Gausmann.)*

Stefan Gausmann, Xiaowen Hu, Jian Zhao, He Cheng, J. E. Antonio-Lopez, Xiaoming Yu, Rodrigo Amezcua-Correa, and Axel Schülzgen are with the CREOL, CREOL, University of Central Florida, Orlando, FL 32816 USA (e-mail: stefan.gausmann@knights.ucf.edu; steven.hu@knights.ucf.edu; jianzhao@knights.ucf.edu; he.cheng@knights.ucf.edu; jealopez@creol.ucf.edu; yux@creol.ucf.edu; r.amezcua@creol.ucf.edu; axel@creol.ucf.edu).

Md. Selim Habib is with the Department of Electrical and Computer Engineering, Florida Polytechnic University, Lakeland, FL 33805 USA (e-mail: mhabib@floridapoly.edu).

Color versions of one or more figures in this article are available at https://doi.org/10.1109/JLT.2022.3229000.

Digital Object Identifier 10.1109/JLT.2022.3229000

II. Chromatic Dispersion in Glass-Air TALOF

The glass-air TALOF used for this work is fabricated in-house at CREOL using the stack and draw technique and has an outer diameter of 452 $\times$ 4 μm and a wall thickness of 73 $\times$ 1 μm leaving a randomized area of roughly 0.11 mm^2. Following the analysis presented in [15], the number of modes supported in the random area of this fiber can be estimated to be on the order of 10^5 for a wavelength of 1 μm. A Scanning electron micrograph (SEM) image of the TALOF facet is shown in Fig. 1(a). The dark regions in the SEM image correspond to air while the bright regions represent fused silica. The air filling fraction across the entire TALOF is roughly 27% and the air hole area distribution extracted from the SEM image has a maximum at

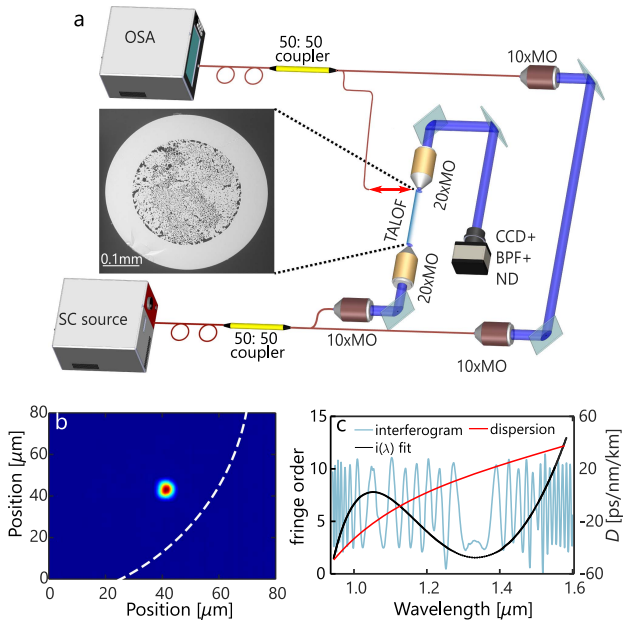

Fig. 1. (a) Illustration of the dispersion balanced Mach-Zender white light interferometer and image acquisition system used to measure the dispersion parameter D and localization length ξ, respectively, of Anderson modes (SC: Supercontinuum, MO: Microscope objective, ND: Neutral density filter, BPF: Band pass filter, OSA: Optical Spectrum Analyzer). (b) Measured near field intensity profile of a highly localized Anderson mode. The dashed white line indicates the position of the TALOF wall in Fig. 1(a). (c) Cyan solid curve: Measured interferogram for the Anderson mode shown in Fig. 1(b). Black solid curve: Fit of the interference fringe order function according to (3). Red solid curve: Dispersion parameter D calculated with (4) from the $i(\lambda)$ fit shown in (c).

4 μm^2 as illustrated in Fig. 7. The random distribution of air holes across the fiber in combination with the varying air hole size and structural invariance in the longitudinal direction, results in strong transverse scattering of light at visible and infrared wavelengths [17] as it propagates through the TALOF and ultimately leads to the formation of Anderson-modes [28], [29]. While the Anderson-modes supported by this type of TALOF can have a wide range of spatial frequencies and extents [4], [17], [28], [29], [30], we focus our study on highly localized Anderson-modes for two reasons: First and foremost because highly localized Anderson modes have demonstrated excellent wave front quality and good broad band transmission properties [14], [15], [17], which makes them in particular interesting for imaging and communication applications. Secondly, such highly localized modes are primarily excited in our experiments launching Gaussian-shaped beams into the TALOF. We solely focused our study on the disordered section of the fiber by exclusively exciting modes that are highly localized and multiple mode sizes separated from the cladding of the fiber. We would like to emphasize that we consider every transversally trapped light state Anderson-localized due to the strong disorder in this fiber. Compared to other binary material TALOFs [26], [31], [32], the constituents of our glass-air TALOF have a rather high refractive index contrast of 1.45, which results in stronger scattering and therefor stronger transverse localization of light. [4], [10].

To measure the chromatic dispersion properties of highly localized Anderson-modes, we placed a 11.7 cm long TALOF sample into the sample-arm of a dispersion balanced Mach-Zender white light interferometer as illustrated in Fig. 1(a). The supercontinuum light is split by a 50:50 fused fiber coupler and launched in the two arms of the interferometer. In the sample arm, the output facet of the broad band fiber coupler is imaged onto the TALOF using a demagnifying 2:1 telescope formed by two microscope objectives. The TALOF is mounted on a high-precision $x-y-z$ translation stage, allowing the excitation of various TALOF modes by scanning the white light beam across the random area. We would like to note, that it was rather easy to excite a large number of different highly localized modes by scanning the TALOF facet across the focused white light beam, which aligns well with observations reported by other groups for similar fibers [14], [15]. A 20 $\times$ microscope objective in combination with a CCD camera and a 10 nm band pass filter (BPF) centered at 1060 nm are used to monitor the transmitted near field intensity profile $I(x, y)$ at the end of the TALOF and to measure the Anderson-mode localization length ξ, defined as [23]:

$$\frac{1}{\xi^2} = \frac{\iint I(x,y)^2\, dx\, dy}{(\iint I(x,y)\, dx\, dy)^2}. \tag{1}$$

We confirmed for each excitation condition that not only the 1060 nm portion but the entire white light spectrum is transversally highly confined in the random structure of the fiber by removing the BPF and monitoring the near field intensity profile before each dispersion measurement. The dispersion proprieties of the excited Anderson-modes are measured by replacing the imaging microscope objective with the bare fiber input of a second 50:50 2 $\times$ 1 fused fiber coupler, which is used to combine the light coming from the reference and sample arm of the interferometer. The length of the reference arm can be adjusted through the length of the free space segment. The dispersion parameter $D(\lambda)$ has been determined by fitting a polynomial function $i(\lambda)$ to the extrema locations of the measured interferogram follwing the method described in Refs. [33], [34], [35], [36] and the Appendix. An example of a measured near field intensity profile of a highly localized Anderson mode is given in Figs. 1(b) and the corresponding interferogram as well as fit function $i(\lambda)$ and dispersion parameter $D(\lambda)$ are shown in Fig. 1(c).

We performed for each highly confined Anderson mode multiple dispersion measurements with slightly modified reference arm lengths and calculated for each Anderson mode the corresponding average dispersion values and standard deviations to estimate the dispersion parameter D as well as the measurement error caused by thermal and mechanical changes of our setup and by imperfections of our fit function. We extracted from the averaged dispersion curves the zero dispersion wavelength (ZDW) as well as the dispersion parameter D at 1.03 μm and 1.55 μm and plotted those important dispersion properties as a function of localization length in Figs. 2(b)–(d).

A clear correlation between the mode size and the dispersion properties of the highly localized Anderson-modes has been observed. Of particular interest is the fact, that the ZDW of

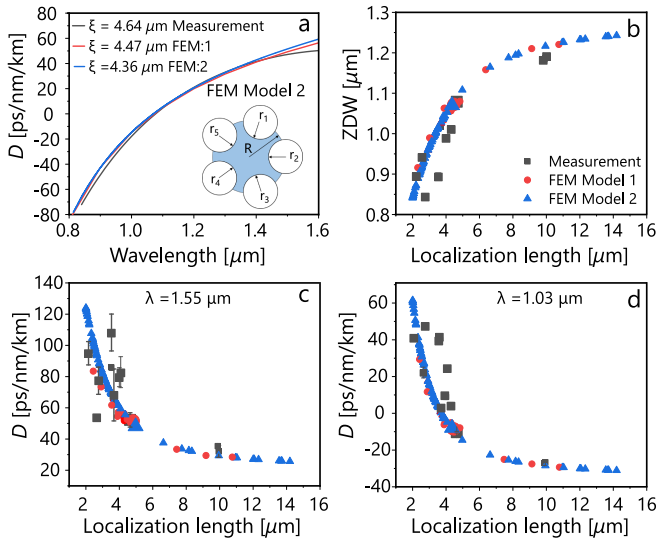

Fig. 2. (a) Comparison between measured (black solid line) and calculated dispersion curves (FEM Model 1: red solid line. FEM Model 2: blue solid line) for Anderson modes with similar mode sizes. The inset represents a sketch of the geometry of FEM Model 2. (b) Comparison of measured (black squares) and calculated zero dispersion wavelength (FEM Model 1: red circles. FEM Model 2: blue triangles) as a function of localization length. (c) & (d) Comparison of measured (black squares) and calculated dispersion parameters D for a wavelength of 1.55 μm and 1.03 μm as a function of localization length (FEM Model 1: red circles. FEM Model 2: blue triangles).

highly localized Anderson modes shifts to shorter wavelength as the localization length decreases due to stronger wave guide dispersion. It should be noted, that this shift exceeds over 300 nm in our TALOF for different localized modes within the same fiber segment. Our measurements also indicate that it is possible to selectively excite highly localized Anderson-modes with anomalous dispersion for wavelengths that are within the emission band of Ti:Sapphire and Ytterbium lasers making this modes highly interesting for pulse compression and nonlinear applications.

To develop a deeper understanding of our experimental findings, we calculated the localized modes guided in random refractive index landscapes as well as their dispersion properties with two different FEM based modelling approaches. The first FEM model, referred to as FEM Model 1, uses the geometry directly extracted from the SEM image in Fig. 1(a) and the material dispersion from Ref. [37] to calculate guided modes and their dispersion properties (details can be found in the Appendix). We considered for our analysis only solutions with large propagation constants and Gaussian-like mode profiles, that remained confined in the same location for wavelengths spanning from 400 nm to 1600 nm, since we selectively excited this subset of highly confined Anderson modes in our experiments. Data obtained by this FEM Model 1 are indicated by red color lines and dots in Fig. 2. The second more generic FEM model, referred to as FEM Model 2, is based on a free-hanging circular silica core geometry with radius R_1 surround by five equally spaced circular air bubbles centered on the air-silica interface with radii $r_{1,\ldots,5}$. A sketch of the FEM Model 2 geometry is illustrated in Fig. 2(a). To account for the randomness of the TALOF used in the experiment, we varied the silica core radius R_1 and the air bubble radii $r_{1,\ldots,5}$ randomly between 3–13 μm and 0.1–0.4 R_1 respectively. We calculated for more than 120 random fiber geometries the dispersion parameter D of the lowest order guided mode as a function of wavelength and the corresponding localization length ξ at a wavelength of 1.06 μm to guaranty a fair comparison to our experiment. FEM Model 2 results are indicated by blue lines and dots in Fig. 2. Our numerical results presented in Figs. 2(a)–(c) show a similar localization length dependency of the dispersion parameter D as our experimental results, even though our measurements seem to agree less well with our simulations for wavelength beyond 1.4 μm. When comparing the good agreement of Model 2 with the experiment all the way from localization length between 2 μm and 10 μm it should be noted that all of these different dispersion properties can be found within the same TALOF segment. In other fiber classes, such as photonic crystal fiber (PCFs), the silica core diameter would have to be varied to achieve such a wide range of dispersion properties. Therefore, if we are looking for specific dispersion properties, we can just scan between different highly localized Anderson-modes supported in a single TALOF instead of having to fabricate multiple fibers with different dimensions. We believe that this new and unique fiber property makes our TALOF an interesting research platform for spatio-temporal effects as well as nonlinear optics.

III. Supercontinuum Generation in Glass-Air TALOF

Motivated by our dispersion measurements, we explore in this section the potential of highly localized Anderson-modes for broad band SC generation in glass-air TALOFs. In order to evaluate which highly localized Anderson-modes are favorable for this particular application, we calculated numerically the spectral width of supercontinua generated in our 11.7 cm short TALOF sample as a function of localization length and pump pulse peak power. We limited our study to Anderson modes with localization length between 2.2 μm and 9.9 μm for two reasons: First, this subset of modes has been primarily observed and was easy to excite during our dispersion measurement. Secondly, this subset covers modes with negative and positive dispersion parameter as well as modes with dispersion parameters close to zero for a pump laser wavelength of 1.03 μm. We modelled the nonlinear pulse propagation along the TALOF by solving the Generalized Nonlinear Schrödinger in the frequency domain using the forth-order Runge-Kutta in the interaction picture (RK4IP) method [38]. Our numerical model includes linear propagation effects such as dispersion and material loss, as well as nonlinear effects such as Kerr-nonlinearity, Raman response, self-steeping and shock-formation in single mode waveguides (details can be found in the Appendix). The wavelength dependent mode area and full dispersion needed for our model have been calculated with FEM Model 2. Fig. 3(a) shows the results of this study for Fourier-limited Gaussian pump pulses with 170 fs FWHM pulse duration, a center wavelength of 1.03 μm and peak powers reaching from 5–70 kW, which are typical values for mode-locked fiber lasers [39]. We found that Anderson-modes with localization lengths smaller than 3 μm are capable

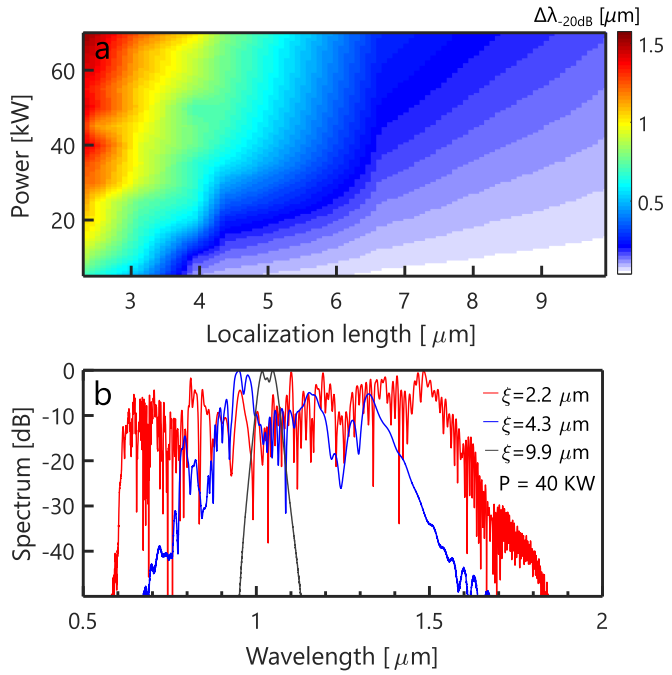

Fig. 3. (a) −20 dB spectral width of supercontinua calculated as a function of pulse peak power for different Anderson localization length in a 11.7 cm short glass-air TALOF. (b) Comparison between SC spectra generated by the same input pulse with 40 kW peak power for three different highly localized Anderson modes in a 11.7 cm short glass-air TALOF.

of generating very broad SC spectra at rather moderate pulse peak powers because those Anderson modes feature anomalous dispersion in the 1 μm wavelength region (see Fig. 2(c)). At the same time, they provide high power densities due to the strong localization. To illustrate the variety of different SC spectra that can be generated within our TALOF by exiting different highly localized Anderson modes with the same pump laser, we show in Fig. 3(b) three calculated SC spectra for highly localized Anderson modes generated by a pulse with 40 kW peak power.

Guided by our previous numerical study, we selectively excited a highly localized Anderson mode with a localization of 2.6 μm and explored experimentally its potential for broad band SC generation using the setup shown in Fig. 4(a). An amplified Yb:KGW laser with 100 kHz repetition rate delivered Fourier limited 170 fs pulses with pulse energies up to a 60 μJ at a center wavelength of 1032 nm and is used as a pump laser for our SC experiments. Neutral density filters and a combination of half wave plates and polarization beam splitters are used to control and reduce the pulse energy to the nJ level (not shown in Fig. 4(a)). A 10 $\times$ microscope objective is utilized to couple the Gaussian laser beam ($M^2 = 1.1$) into the previously characterized 11.7 cm long silica TALOF sample. The TALOF is mounted on a high-precision $x - y - z$ translation stage, allowing different Anderson-modes at different locations across the TALOF to be excited. A 20 $\times$ microscope objective in combination with a 10 nm wide band pass filter centered at 1030 nm and a CCD camera are used to monitor near field intensity distribution at the end faced of the TALOF, to ensure the excitation of highly localized Anderson modes and to measure the localization length of the excited Anderson mode. The spectrum of the pulses after propagation through the TALOF has been measured by replacing the 20 $\times$ microscope objective with a 0.7 m long large core step index fiber with a core diameter of 105 μm and a core numerical aperture of 0.22, which was connected to an Optical Spectrum Analyzer (OSA). The coupling efficiency into the highly localized Anderson mode has been measured by monitoring the power ratio measured before the 10 $\times$ microscope objective and at the end of the TALOF after passing through an aperture, which has been used to block the scattered light that is not launched into the highly localized Anderson-mode. Fig. 4(b) shows three SC spectra generated by coupling differently attenuated pump pulses into the highly localized Anderson mode with a localization length of $\sim$2.6 μm. The launching efficiency into this mode, which is defined as the average power exiting the fiber divided by the average power launched into the fiber, has been measured to be 33%. The measured near field intensity distribution of this mode is shown in the inset in Fig. 4(g). Fig. 2(b) shows that at the highest launched peak power of 70 kW, the generated SC reaches from 462 nm to 1750 nm using the –20 dB level as a reference. Coupling higher peak powers into this highly confined Anderson-mode resulted in irreversible beam degradation most likely caused by fiber damage.

To better understand our measured SC spectra and the enabling generation mechanisms, we compared our measurement results to numerical simulations. The wavelength dependent mode area and full dispersion needed for our model have been calculated with FEM Model 2 for a random refractive index landscape with a fundamental mode localization length close to the one we measured in our experiment and are shown in Fig. 4(g). Pulse parameters, such as pulse peak power, pulse duration and chirp as well as the pulse center wavelength used in our model correspond to the pulse parameters of the experiment to ensure fair comparison. In order to account for quantum noise and the relative intensity noise of our pump laser, we added 1.5% peak power fluctuation and one photon with random phase noise per frequency channel to the input pulse of our simulation and averaged over 20 single shot SC simulations when comparing our experimental data with the simulations in Fig. 4(b). A detailed description of the used SC model and measurement error corrections can be found in the Appendix.

Fig. 4(c), (d) show the temporal and spectral dynamics of the SC generation process along the fiber for a pulse with 15 kW peak power. During the initial $\sim$3 cm of propagation, the launched pump pulse undergoes soliton self-compression, which manifests itself by significant pulse compression in the time domain and spectral broadening in the frequency domain [40]. Our simulations indicate a peak power enhancement factor of $\sim$8 and FWHM pulse duration as short as 6 fs for input pulse with 170 fs pulse duration and 15 kW peak power during this process. Higher order dispersion and the nonlinear Raman response perturb the periodic higher order soliton evolution in the fiber and cause the ejection of multiple solitons [41]. The ejected solitons separate in time from the initial pulse by different amounts due to group-velocity walk-off and red shift in the frequency domain due to soliton self-frequency shifts [40], [42]. The frequency

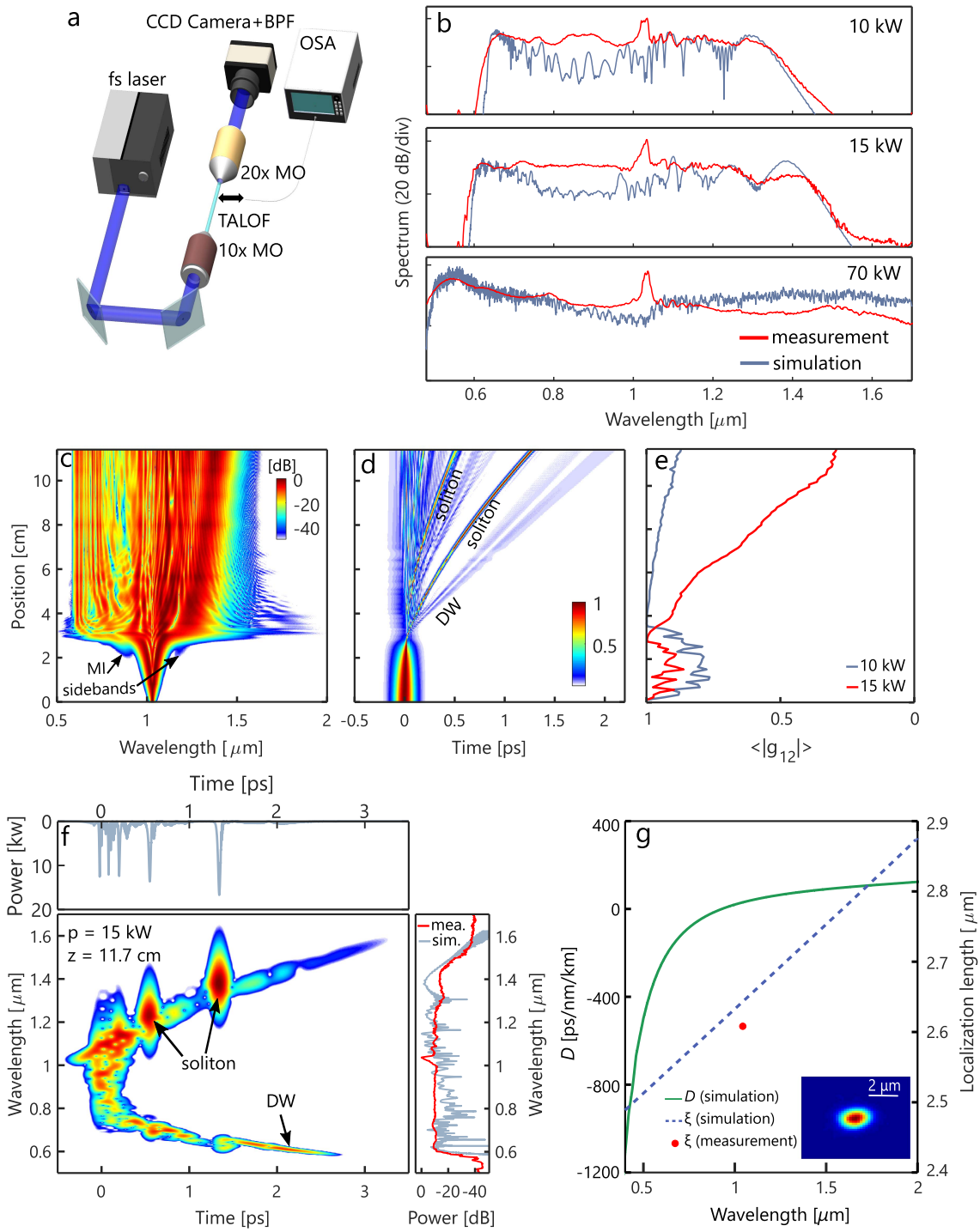

Fig. 4. (a) Experimental setup used for SC generation in TALOF. (b) Comparison between measured (red solid line) and calculated (grey solid line) supercontinuum spectra for input peak powers of 10 kW, 15 kW and 70 kW propagating through 11.7 cm TALOF in a strongly localized mode with localization length of 2.6 μm. (c) & (d) Calculated spectral and temporal SC evolution along the fiber for an input pulse with 15 kW peak power.(e) Evolution of spectrally averaged coherence calculated for 20 single shot simulations with 10 kW (grey solid curve) and 15 kW (red solid curve) peak power.(f) Calculated spectrogram of single shot simulation for an input pulse with 15 kW peak power at $z = 11.7$ cm. (g) Calculated dispersion parameter D (green solid line) and Anderson localization length (blue dashed line) used for SC simulations. Inset: Measured near field intensity distribution of the Anderson mode excited for the SC experiment.

shifted solitons and their phase-matched dispersive waves (DW) on the short wavelength side of the spectrum define upper and lower spectral limit of the generated SC at the end of the fiber as the spectrogram calculated at $z = 11.7$ cm illustrates in Fig. 4(f). Our simulations predict the extend of the generated SC as well as the location of spectral features such as the position of the first ejected soliton during the soliton fission process fairly well. The peak at the pump wavelength in the measured SC spectra is not apparent in our simulations and is most likely caused by the collection of scattered light, as the coupling efficiency of

the pump laser into the highly localized Anderson mode was far from perfect and the core size of the collection fiber was much larger than the highly localized Anderson mode.

The coherence properties of the generated supercontinua have been investigated numerically by calculating the modulus of the complex degree of first order coherence at zero path difference defined as [41], [43], [44], [45], [46]:

$$|g_{12}(\lambda)| = \left| \frac{< S_1^*(\lambda) S_2(\lambda) >}{\sqrt{< |S_1(\lambda)|^2 >< |S_2(\lambda)|^2 >}} \right|, \qquad (2)$$

where the angled brackets indicate the ensemble average over independently generated complex SC spectra $[S_1, S_2]$ evaluated for 20 independent single shot simulations, respectively. The spectrally averaged coherence $< |g_{12}| >$ has been determined by weighting $|g_{12}|$ with the averaged spectrum of the corresponding ensemble [43]. While $< |g_{12}| >$ with values close to 1 indicates a good spectral amplitude and phase stability for peak powers below 10 kW, a sharp drop in coherence is observed for peak powers above 10 kW as shown in Fig. 6. Whereas $< |g_{12}| >$ evolves similar for 10 kW and 15 kW peak power pulses at the beginning of the fiber, a significant coherence degradation is observed after pulse self-compression and during the soliton fission process for the 15 kW peak power case, while the coherence for the 10 kW peak power case remains almost constant along the fiber as shown in Fig. 4(e). The loss of spectrally averaged coherence goes hand in hand with strong time jitter of the ejected solitons as shown in the Fig. 6. This degradation of coherence is typically attributed to the amplification of input noise by phase-matched four wave mixing (FWM) resulting in a non-deterministic soliton fission process and therefore a loss of coherence and a gain in timing jitter at the end of the fiber [41]. We believe that this argument applies for our study as well as Modulation Instability (MI) sidebands, which result from noise amplification due to degenerated FWM, start to appear for peak powers above 10 kW and seed the soliton fission process as highlighted in Fig. 4(c).

The broad band SC generation discussed above is just one example of applications, for which the tunable dispersion properties of highly localized TALOF modes can be advantageous for. It should be noted that the same short piece of TALOF and the same pump laser can be utilized to generate supercontinua with a variety of different spectral and temporal features or coherence properties depending on which highly localized Anderson mode is excited. In addition, the widely tunable ZDW allows for a large flexibility in choosing the pump laser wavelength for SC generation, which is a clear advantage of our glass-air TALOF compared to conventional photonic crystal fibers for example, where a change in fiber geometry is required to fundamentally change the dispersion properties and therefore SC generation process. TALOFs are highly multimode systems like conventional step index multimode fibers with the key difference that guided modes in TALOFs can be spatially isolated due to the strong disorder and do not cover the entire guiding region of the fiber. Therefore, we believe that our glass-air TALOFs might also be a promising test system for novel spatio temporal and pulse compression applications.

IV. Conclusion

In conclusion, we experimentally and numerically explored the dispersion properties of highly localized Anderson-modes in a disordered glass-air fiber and exploited these unique mode properties to demonstrate broad band supercontinuum generation in a short segment of TALOF. Our dispersion measurements reveal a clear correlation between the Anderson localization length and the dispersion properties for highly localized of Anderson-modes. Our measurements and simulations indicate that the ZDW of highly localized TALOF modes can be tuned between 840 and 1150 nm by simply exciting an Anderson-mode with a different localization length. We further demonstrated multi octave spanning SC ranging from 460–1750 nm. We hope that our results, will help further understanding of light propagation in disordered waveguides and pave the way for new application of TALOFs in highly relevant areas such as nonlinear fiber optics and fiber communications.

Appendix

This appendix provides supplementary information to 'Tunable dispersion and supercontinuum generation in disordered glass-air Anderson localization fiber'. We discuss here the FEM Model#1, which has been used to validated our dispersion measurements, as well as the numerical pulse propagation model, which has been used to validate our supercontinuum (SC) experiments. We further discuss the methods used to extract the dispersion parameter D of highly localized Anderson modes from our dispersion measurements and the statistic distribution of air holes in our transversal Anderson localization optical fiber (TALOF).

A. Dispersion Measurement of TALOF

A sketch and detailed description of the dispersion balanced Mach-Zenderwhite light interferometer used to measure the dispersion properties of highly localized Anderson modes can found in the second section of the main document. The spectral phase difference between the two interferometer arms induced by the TALOF has been extracted from the interferogram by counting the order of the maxima and minima, and assigning the corresponding wavelength positions [33], [34], [35], [36]. For a bright fringe in the spectral interferogram, the optical path difference between the two interferometer arms has to satisfy:

$$L - l - n(\lambda_i) z = (m + i)\lambda_i, \qquad (3)$$

where L is length of the reference arm, l is the length of the sample arm without fiber, i is the interference order, m is an arbitrary integer, λ_i is the wavelength position associated with the ith interference fringe, z is TALOF segment length and $n(\lambda)$ is the wavelength depended refractive index of the fiber to be measured. A similar relation can be derived for the dark fringes of the spectral interferogram.

The dispersion parameter D has been determined by assuming the modified Cauchy dispersion formula for $n(\lambda)$ and fitting a

polynomial of the form:

$$i(\lambda) = a_1\lambda^{-5} + a_2\lambda^{-3} + a_3\lambda^{-1} + a_4\lambda + a_5\lambda^3 - m \quad (4)$$

to the interference fringe order function (λ_i) and subsequently calculating the dispersion parameter D using:

$$D(\lambda) = \frac{1}{c_0 z}(20a_1\lambda^{-5} + 6a_2\lambda^{-3} + 2a_4\lambda + 12a_5\lambda^3), \quad (5)$$

where c_0 is the speed of light in vacuum and $a_j (j = 1, 2, 4, 5)$ are fitting parameters from the above dispersion equation [33], [34], [35], [36]. Examples of $i(\lambda)$ and $D(\lambda)$ are shown together with the measured interferogram in Fig. 1(c) of the main document.

B. Details of the FEM Model#1

In this section we describe the FEM Model#1, which has been used to calculate the localization length ξ and the dispersion parameter D of highly localized Anderson modes in our glass-air TALOF. The geometries for our FEM simulations are directly imported from the scanning electron micrograph (SEM) image to COMSOL Multiphysics. As the feature sizes of the air bubbles in the random region of our TALOF is rather small compared to the total size of the fiber, intense meshing would be required to find guided modes across the entire structure. To make our study computationally less intensive, we searched only in small sections of the fiber for modes as shown in Figs. 5(a, b).

Fig. 5(b) shows the near field intensity profiles of three different modes that have calculated for the geometry highlighted by a red circle in Fig. 5(a). We considered for our analysis only solutions with large propagation constants and Gaussian-like mode profiles, that remained confined in the same location for wavelengths spanning from 400 nm to 1600 nm. The dispersion parameter D at a wavelength λ has been calculated from the effective refractive index of a specific mode using the material dispersion from [37] and:

$$D(\lambda) = -\frac{\lambda}{c_0}\frac{n_{\text{eff}}(\lambda + \Delta\lambda) - 2n_{\text{eff}}(\lambda) + n_{\text{eff}}(\lambda - \Delta\lambda)}{\Delta\lambda^2}, \quad (6)$$

where c_0 corresponds to the speed of light in vacuum and $\Delta\lambda$ corresponds to a small deviation from λ. Figs. 5(c) and (d) show the calculated dispersion D near the zero dispersion wavelength as well as the calculated localization length as a function of wavelength for the three modes shown in Fig. 5(b).

C. Numerical Modeling of SC and Collection Loss Correction for Comparison With Experimental Results

The optical pulse propagation in the glass-air TALOF was numerically calculated by solving the Generalized Nonlinear Schrödinger Equation (GNLSE) in the frequency domain of the form [47]:

$$\frac{\partial\widetilde{C}}{\partial z} - i\left(\beta(\omega) - \beta(\omega_0) - \beta_1(\omega_p)[\omega - \omega_0] + i\frac{\alpha(\omega)}{2}\right)$$

$$\widetilde{C}(z,\omega) = i\gamma\left(1 + \frac{\omega - \omega_0}{\omega_0}\right)\mathcal{F}\left\{\int_{-\infty}^{t} R(t')|C(z, t - t')|^2\, dt'\right\}, \quad (7)$$

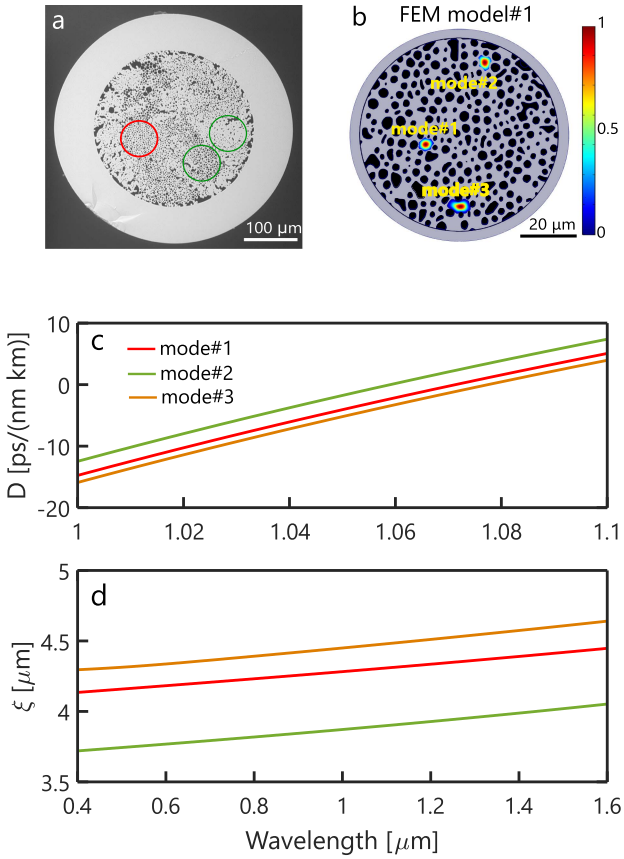

Fig. 5. (a) SEM image of TALOF investigated in this study. The circles indicate domains used for our dispersion study. (b) Intensity profile of three highly localized modes calculated for the domain within the red circle (a). (c) Calculated dispersion D and (d) localization length ξ as a function of wavelength for the modes shown in shown in (b).

where $\beta(\omega)$ is the wavelength dependent full propagation constant, $\beta(\omega_0)$ is propagation constant at center frequency, ω_0, $\beta_1(\omega_p)$ is the inverse of group velecocity, v_g at pump frequency, ω_p, $\alpha(\omega)$ is the fiber attenuaiton in m^{-1}, and C is the Fourier transform of $\widetilde{A}(z,\omega) = \mathcal{F}\{A(z,t)\}$ of the field envelop $A(z,t)$ related to [48]:

$$\mathcal{F}\{C(z,t)\} = \widetilde{C}(z,\omega) = \left[\frac{\xi^2(\omega)}{\xi^2(\omega_0)}\right]^{-\frac{1}{4}} A(z,\omega), \quad (8)$$

where $\xi^2(\omega)$ is the wavelength dependent effective mode area of the fiber and the nonlinear coefficient $\gamma(\omega)$ can be expressed as [48]:

$$\gamma(\omega) = \frac{n_2 n_0 \omega_0}{c_0 n_{\text{eff}}(\omega)\sqrt{\xi^2(\omega)\xi^2(\omega_0)}}, \quad (9)$$

where n_{eff} is the wavelength dependent effective mode index, ω_0 is the center frequency, $n_2 = 2.7 \times 10^{-20}$ m^2/W [49] is the nonlinear refractive index and ξ^2 is the effective mode area. The Raman response function $R(t) = (1 - f_R)\delta(t) + f_R h_r(t)$ includes the instantaneous electronic as well as delayed response function which has be approximated by [50]:

$$h_r(t) = f_a\frac{\tau_1^2}{\tau_1^2 + \tau_2^2}e^{-\frac{t}{\tau_2}}\sin\left(\frac{t}{\tau_1}\right), \quad (10)$$

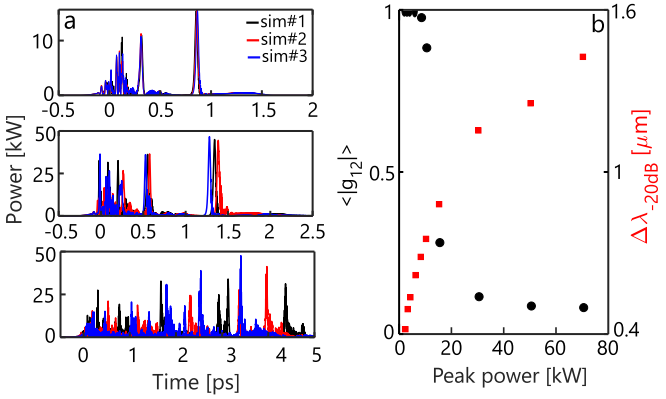

Fig. 6. (a) Temporal profile of the TALOF at the end of fiber for different single shot simulations and peaks powers. (b) Spectrally averaged coherence (black circles) and −20 dB spectral width (red squares) as a function of peak power calculated for ensembles of 20 single shot simulations.

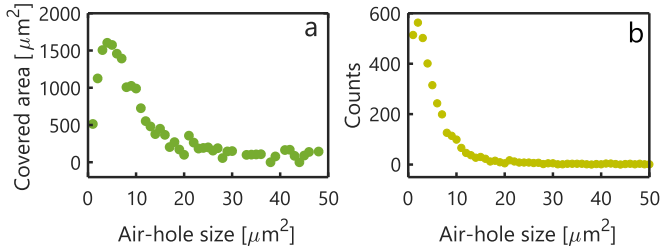

Fig. 7. (a) Covered area by specific hole size across the random area of the TALOF shown in Fig. 1(a). (b) Number of air holes of certain size across the random area of the TALOF shown in Fig. 5(a).

where $\tau_1 = 12.2$ fs, $\tau_2 = 32$ fs and $f_a = 0.75$. The material loss used for our simulations corresponds to Heraeus F300HQ glass [51]. To account for pulse to pulse peak power fluctuation (PPPF) of the pump laser as well as for quantum noise, we added a random PPPF of 1.5%, as specified by the laser manufacturer, and one photon per frequency channel with random phase to the input pulse and averaged 20 single shot simulations for each curve shown in Fig. 4(b) of the main document. Fig. 6(a), (b) show the the timing jitter at the end of TALOF for three different single shot simulations and the spectrally averaged coherence as well as the −20 dB spectral width of the generated SC calculated from 20 single shot simulations for the pulse and Anderson mode parameters discussed in the main document.

As the far-field divergence angle $\theta = \lambda/(\sqrt{\pi}\xi(\lambda))$ of the highly localized Anderson mode studied in our experiment exceeds the numerical aperture of our collection step index fiber for wavelength longer than $\tilde{1}000$ nm, we modified the averaged simulation spectra shown in Fig. 4(b) of the main manuscript by a wavelength dependent collection loss term, which we calculated with the Fraunhofer diffraction integral, $\text{Loss}(\lambda) = 1 - e^{-2\frac{\Theta(\lambda)}{NA}}$, where θ is the far field divergence angle of the Anderson mode and NA is numerical aperture of the collection fiber. We further included the NA dependent level correction provided by optical spectrum analyzer (OSA) manufacturer [52], when comparing our experimental data with our numerical simulations in Fig. 4(b) of the main manuscript.

D. Air Hole Statistics

The glass-air TALOF used for this study has been drawn in house at CREOL using the stack and draw technique. The geometrical properties of this fiber have been characterized using the Scanning Electron Microscopy (SEM) image shown in Fig. 5(a) and the open source image analysis tool ImageJ [53]. Fig. 7(a) and (b) show the statistical hole area distribution across the TALOF in therms of covered area and their appearance as a function air hole size. Even though the most common air hole size peaks at 2 μm, the most area is covered by air holes at 4 μm. The air filling fraction across the entire random area of fiber roughly 27%.

REFERENCES

[1] S. Abdullaev and F. K. Abdullaev, "On propagation of light in fiber bundles with random parameters," *Radiofizika*, vol. 23, no. 6, pp. 766–767, 1980.
[2] H. De Raedt, A. Lagendijk, and P. de Vries, "Transverse localization of light," *Phys. Rev. Lett.*, vol. 62, no. 1, pp. 47–50, 1989.
[3] M. Störzer, P. Gross, C. M. Aegerter, and G. Maret, "Observation of the critical regime near anderson localization of light," *Phys. Rev. Lett.*, vol. 96, no. 6, 2006, Art. no. 063904.
[4] A. Mafi, "Transverse anderson localization of light: A tutorial," *Adv. Opt. Photon.*, vol. 7, no. 3, pp. 459–515, 2015.
[5] M. Segev, Y. Silberberg, and D. N. Christodoulides, "Anderson localization of light," *Nature Photon.*, vol. 7, no. 3, pp. 197–204, 2013.
[6] M. Koirala, R. Sarma, H. Cao, and A. Yamilov, "Inverse design of perfectly transmitting eigenchannels in scattering media," *Phys. Rev. B*, vol. 96, no. 5, 2017, Art. no. 054209.
[7] A. P. Mosk, A. Lagendijk, G. Lerosey, and M. Fink, "Controlling waves in space and time for imaging and focusing in complex media," *Nature Photon.*, vol. 6, no. 5, p. 283–292, 2012.
[8] A. Chabanov, M. Stoytchev, and A. Genack, "Statistical signatures of photon localization," *Nature*, vol. 404, no. 6780, pp. 850–853, 2000.
[9] S. Karbasi, C. R. Mirr, P. G. Yarandi, R. J. Frazier, K. W. Koch, and A. Mafi, "Observation of transverse anderson localization in an optical fiber," *Opt. Lett.*, vol. 37, no. 12, pp. 2304–2306, 2012.
[10] S. Karbasi, C. R. Mirr, R. J. Frazier, P. G. Yarandi, K. W. Koch, and A. Mafi, "Detailed investigation of the impact of the fiber design parameters on the transverse anderson localization of light in disordered optical fibers," *Opt. Exp.*, vol. 20, no. 17, pp. 18692–18706, 2012.
[11] S. Karbasi, T. Hawkins, J. Ballato, K. W. Koch, and A. Mafi, "Transverse anderson localization in a disordered glass optical fiber," *Opt. Mater. Exp.*, vol. 2, no. 11, pp. 1496–1503, 2012.
[12] M. Chen and M.-J. Li, "Observing transverse anderson localization in random air line based fiber," *SPIE*, vol. 8994, 2014, Art. no. 89941S.
[13] J. Zhao et al., "Image transport through meter-long randomly disordered silica-air optical fiber," *Sci. Rep.*, vol. 8, no. 1, pp. 1–7, 2018.
[14] G. Ruocco, B. Abaie, W. Schirmacher, A. Mafi, and M. Leonetti, "Disorder-induced single-mode transmission," *Nature Commun.*, vol. 8, no. 1, pp. 1–6, 2017.
[15] B. Abaie et al., "Disorder-induced high-quality wavefront in an anderson localizing optical fiber," *Optica*, vol. 5, no. 8, pp. 984–987, 2018.
[16] W. Schirmacher, B. Abaie, A. Mafi, G. Ruocco, and M. Leonetti, "What is the right theory for anderson localization of light? an experimental test," *Phys. Rev. Lett.*, vol. 120, no. 6, 2018, Art. no. 067401.
[17] P. Roth et al., "Wavelength dependence of transverse anderson localization in disordered glass-air fiber," in *Proc. 6th Int. Workshop Specialty Opt. Fibers Their Appl.*, 2019, vol. 11206, Art. no. 112061M–1.
[18] S. Karbasi, R. J. Frazier, K. W. Koch, T. Hawkins, J. Ballato, and A. Mafi, "Image transport through a disordered optical fibre mediated by transverse anderson localization," *Nature Commun.*, vol. 5, no. 1, pp. 1–9, 2014.
[19] T. H. Tuan, S. Kuroyanagi, K. Nagasaka, T. Suzuki, and Y. Ohishi, "Near-infrared optical image transport through an all-solid tellurite optical glass rod with transversely-disordered refractive index profile," *Opt. Exp.*, vol. 26, no. 13, pp. 16054–16062, 2018.

[20] A. Mafi, J. Ballato, K. W. Koch, and A. Schülzgen, "Disordered anderson localization optical fibers for image transport–A review," *J. Lightw. Technol.*, vol. 37, no. 22, pp. 5652–5659, 2019.
[21] J. Zhao et al., "Deep-learning cell imaging through anderson localizing optical fiber," *Adv. Photon.*, vol. 1, no. 6, 2019, Art. no. 066001.
[22] M. Leonetti, S. Karbasi, A. Mafi, and C. Conti, "Light focusing in the anderson regime," *Nature Commun.*, vol. 5, no. 1, pp. 1–6, 2014.
[23] M. Leonetti et al., "Experimental observation of disorder induced self-focusing in optical fibers," *Appl. Phys. Lett.*, vol. 105, no. 17, 2014, Art. no. 171102.
[24] M. Leonetti, S. Karbasi, A. Mafi, E. DelRe, and C. Conti, "Secure information transport by transverse localization of light," *Sci. Rep.*, vol. 6, no. 1, pp. 1–7, 2016.
[25] B. Abaie, E. Mobini, S. Karbasi, T. Hawkins, J. Ballato, and A. Mafi, "Random lasing in an anderson localizing optical fiber," *Light: Sci. Appl.*, vol. 6, no. 8, pp. e17041–e17041, 2017.
[26] M. Tuggle, C. Bassett, T. W. Hawkins, R. Stolen, A. Mafi, and J. Ballato, "Observation of optical nonlinearities in an all-solid transverse anderson localizing optical fiber," *Opt. Lett.*, vol. 45, no. 3, pp. 599–602, 2020.
[27] G. P. Agrawal, *Fiber-Optic Communication Systems*, vol. 222. Hoboken, NJ, USA: Wiley, 2012.
[28] R. G. El-Dardiry, S. Faez, and A. Lagendijk, "Snapshots of anderson localization beyond the ensemble average," *Phys. Rev. B*, vol. 86, no. 12, 2012, Art. no. 125132.
[29] Y. Lahini et al., "Anderson localization and nonlinearity in one-dimensional disordered photonic lattices," *Phys. Rev. Lett.*, vol. 100, no. 1, 2008, Art. no. 13906.
[30] P. Sebbah, B. Hu, J. M. Klosner, and A. Z. Genack, "Extended quasimodes within nominally localized random waveguides," *Phys. Rev. Lett.*, vol. 96, no. 18, 2006, Art. no. 183902.
[31] S. Karbasi, R. J. Frazier, C. R. Mirr, K. W. Koch, and A. Mafi, "Fabrication and characterization of disordered polymer optical fibers for transverse anderson localization of light," *J. Visualized Exp.: JoVE*, no. 77, 2013, Art. no. e50679.
[32] T. H. Tuan, S. Kuroyanagi, K. Nagasaka, T. Suzuki, and Y. Ohishi, "Characterization of an all-solid disordered tellurite glass optical fiber and its NIR optical image transport," *Japanese J. Appl. Phys.*, vol. 58, no. 3, 2019, Art. no. 32005.
[33] J. Knight, J. Arriaga, T. Birks, A. Ortigosa-Blanch, W. Wadsworth, and P. S. J. Russell, "Anomalous dispersion in photonic crystal fiber," *IEEE Photon. Technol. Lett.*, vol. 12, no. 7, pp. 807–809, Jul. 2000.
[34] U. Møller et al., "Multi-milliwatt mid-infrared supercontinuum generation in a suspended core chalcogenide fiber," *Opt. Exp.*, vol. 23, no. 3, pp. 3282–3291, 2015.
[35] P. Ciąćka, A. Rampur, A. Heidt, T. Feurer, and M. Klimczak, "Dispersion measurement of ultra-high numerical aperture fibers covering thulium, holmium, and erbium emission wavelengths," *J. Opt. Soc. Amer. B*, vol. 35, no. 6, pp. 1301–1307, 2018.
[36] P. Hlubina, M. Kadulová, and P. Mergo, "Chromatic dispersion measurement of holey fibres using a supercontinuum source and a dispersion balanced interferometer," *Opt. Lasers Eng.*, vol. 51, no. 4, pp. 421–425, 2013.
[37] J. W. Fleming, "Dispersion in GEO 2–SIO 2 glasses," *Appl. Opt.*, vol. 23, no. 24, pp. 4486–4493, 1984.
[38] A. Rieznik, A. M. Heidt, P. Konig, V. A. Bettachini, and D. Grosz, "Optimum integration procedures for supercontinuum simulation," *IEEE Photon. J.*, vol. 4, no. 2, pp. 552–560, Apr. 2012.
[39] A. Chong, W. H. Renninger, and F. W. Wise, "All-normal-dispersion femtosecond fiber laser with pulse energy above 20NJ," *Opt. Lett.*, vol. 32, no. 16, pp. 2408–2410, 2007.
[40] G. P. Agrawal, "Nonlinear fiber optics," in *Nonlinear Science at the Dawn of the 21st Century*. Heidelberg, Germany: Springer, 2000, pp. 195–211.
[41] J. M. Dudley, G. Genty, and S. Coen, "Supercontinuum generation in photonic crystal fiber," *Rev. Modern Phys.*, vol. 78, no. 4, 2006, Art. no. 1135.
[42] J. P. Gordon, "Theory of the soliton self-frequency shift," *Opt. Lett.*, vol. 11, no. 10, pp. 662–664, 1986.
[43] J. M. Dudley and S. Coen, "Coherence properties of supercontinuum spectra generated in photonic crystal and tapered optical fibers," *Opt. Lett.*, vol. 27, no. 13, pp. 1180–1182, 2002.
[44] M. S. Habib, C. Markos, O. Bang, and M. Bache, "Soliton-plasma nonlinear dynamics in mid-Ir gas-filled hollow-core fibers," *Opt. Lett.*, vol. 42, no. 11, pp. 2232–2235, 2017.
[45] A. I. Adamu et al., "Deep-UV to mid-IR supercontinuum generation driven by mid-IR ultrashort pulses in a gas-filled hollow-core fiber," *Sci. Rep.*, vol. 9, no. 1, pp. 1–9, 2019.
[46] A. I. Adamu et al., "Noise and spectral stability of deep-UV gas-filled fiber-based supercontinuum sources driven by ultrafast mid-Ir pulses," *Sci. Rep.*, vol. 10, no. 1, pp. 1–10, 2020.
[47] M. H. Frosz, "Validation of input-noise model for simulations of supercontinuum generation and rogue waves," *Opt. Exp.*, vol. 18, no. 14, pp. 14778–14787, 2010.
[48] J. Laegsgaard, "Mode profile dispersion in the generalized nonlinear schrödinger equation," *Opt. Exp.*, vol. 15, no. 24, pp. 16110–16123, 2007.
[49] D. Milam, "Review and assessment of measured values of the nonlinear refractive-index coefficient of fused silica," *Appl. Opt.*, vol. 37, no. 3, pp. 546–550, 1998.
[50] Q. Lin and G. P. Agrawal, "An accurate model for the raman response function in silica fibers," in *Proc. IEEE Conf. Lasers Electro- Opt. Quantum Electron. Laser Sci. Conf.*, 2006, pp. 1–2.
[51] Heraeus, [Online]. Available: http://www.heraeus.com
[52] Yokogawa, *AQ6374Optical Spectrum Analyzer User's Manual*.
[53] W. S. Rasband, "National institutes of health, Bethesda, Maryland, USA," 2011. [Online]. Available: http://imagej.nih.gov/ij/

Stefan Gausmann received the B.S. and M.S. degrees in physics from RWTH Aachen University, Aachen, Germany, in 2014 and 2016, respectively, the second M.S. degree in 2017, and the Ph.D. degree in optics and photonics from the University of Central Florida, Orlando, FL, USA, in 2021. His research interests include high power CW fiber lasers and nonlinear optics.

Xiaowen Hu received the B.S. degree in optical science and technology from Fudan University, Shanghai, China, China, in 2015. He is currently working toward the Ph.D. degree in optics and photonics with CREOL, The College of Optics and Photonics, University of Central Florida, Orlando, FL, USA. His research interests include microstructured fiber optics, machine learning applications in optics, and optical fiber imaging.

Jian Zhao received the B.S. degree in optics from the School of Physics and Engineering, Sun Yat-sen University, Guangzhou, China, and the Ph.D. degree in optics and photonics from CREOL, the College of Optics and Photonics from the University of Central Florida, Orlando, FL, USA. He is currently a Postdoctoral Researcher with the Picower Institute, Cambridge, MA, USA, with the Massachusetts Institute of Technology, Cambridge, MA, USA. Before joining the Picower Institute, he was a Postdoctoral Associate Affiliated with the Department of Electrical and Computer Engineering with Boston University, Boston, MA, USA. He is a Member of SPIE and OSA. His research interests include label-free chemical computational microscopy, mid-infrared photothermal microscopy, multiphoton microscopy, deep learning in optics, microstructured optical fibers, and ultrafast optics.

Md. Selim Habib (Senior Member, IEEE) received the B.Sc. and M.Sc. degrees in electrical and electronic engineering from the Rajshahi University of Engineering and Technology, Rajshahi, Bangladesh, in 2008 and 2012, respectively, and the Ph.D. degree in photonics engineering from the Technical University of Denmark (DTU), Kongens Lyngby, Denmark, in 2017. After finishing his Ph.D., he joined as a Postdoctoral Researcher in Fibers Sensors and Supercontinuum Group with the Department of Photonics Engineering, DTU. After finishing his Postdoctoral Fellowship with DTU, he was a Postdoctoral Research Associate with CREOL, The College of Optics and Photonics, University of Central Florida, Orlando, FL, USA, from September 2017 to August 2019. He is currently an Assistant Professor of electrical and computer engineering with Florida Polytechnic University. He has authored or coauthored more than 40 articles in referred journals. His research interests include design, fabrication, and characterization of low loss hollow-core fiber in the near-IR to mid-IR, light gas nonlinear interaction in hollow-core fibers, supercontinuum generation, and multi-mode nonlinear optics. He is a Senior Member of the Institute of Electrical and Electronics Engineers (IEEE) and Optica, and Executive officer of Optica Fiber modeling and Fabrication group. He is an Associate Editor for the IEEE ACCESS, and Feature Editor of *Applied Optics* (OSA). He was the recipient of the the University Gold Medal Award from Rajshahi University of Engineering and Technology in 2014.

He Cheng biography not available at the time of publication.

J. E. Antonio-Lopez received the Ph.D. degree from the Instituto Nacional de Astrofísica, Óptica y Electrónica (INAOE), San Andres Cholula, Mexico, in 2012, with the work design and fabrication of photonic devices based on multimode interference. He is a Research Scientist with the College of Optics and Photonics (CREOL), University of Central Florida, Orlando, FL, USA. His research interests include design, fabrication, and use of special fibers.

Xiaoming Yu received the B.S. degree in physics from Nankai University, Tianjin, China, in 2008, the M.S. degree in plasma physics from the Shanghai Institute of Optics and Fine Mechanics, Shanghai, China, in 2012, and the Ph.D. degree in industrial and manufacturing systems engineering from Kansas State University, Manhattan, KS, USA, in 2016. His research interest include laser-matter interaction and laser-based advanced manufacturing.

Rodrigo Amezcua-Correa (Member, IEEE) received the Ph.D. degree from Optoelectronics Research Centre (ORC) from the University of Southampton, Southampton, U.K. in 2009. Since 2011, he has been with the College of Optics and Photonics, University of Central Florida, Orlando, FL, USA, where he currently is an Associate Professor of optics and photonics. His research interests include fiber design and fabrication for applications including communications, fiber lasers, nonlinear optics, and sensing.

Axel Schülzgen (Fellow, IEEE) received the Ph.D. degree in physics from the Humboldt-University of Berlin, Berlin, Germany. Since 2009, he has been a Professor of optics and photonics with CREOL, The College of Optics and Photonics, University of Central Florida, Orlando, FL, USA. He also holds an Adjunct Research Professor position with the College of Optical Sciences, University of Arizona, Tucson, AZ, USA. He authored more than 130 scientific publications in peer reviewed journals, more than 60 invited talks at international conferences, and six patents. His research interests include optical fiber devices, components, materials, and structures with applications in fiber laser systems, fiber optic sensing and imaging, and optical communications. He is a Fellow of the Optical Society of America.